Absolute measurements of electron-loss cross sections of He^+ and C^{3+} with atomic hydrogen at intermediate velocities

M. M. Sant'Anna,* W. S. Melo,* A. C. F. Santos, G. M. Sigaud, and E. C. Montenegro
Departamento de Física, Pontifícia Universidade Católica do Rio de Janeiro, Caixa Postal 38071, Rio de Janeiro 22452-970, Brazil

M. B. Shah
Department of Pure and Applied Physics, The Queen's University of Belfast, Belfast BT7 1NN, Northern Ireland, United Kingdom

W. E. Meyerhof
Department of Physics, Stanford University, Stanford, California 94305-4060
(Received 28 January 1998)

Cross sections for electron loss of He^+ and C^{3+} projectile ions on atomic and molecular hydrogen were measured in the 0.5-MeV$\leqslant E \leqslant$3.5-MeV energy range. The measurements of the σ_{H_2}/σ_H cross section ratios were made by using an absolutely calibrated hydrogen furnace. The influence of different models describing the form factor of molecular hydrogen is examined by means of the ratio σ_{H_2}/σ_H, which is sensitive to the model adopted, particularly in the case of He^+ projectiles. The general behavior of the measured data is analyzed within the independent electron approximation including the electron loss (screening and antiscreening contributions), electron capture, and target ionization channels. The connection between the antiscreening mode and the electron impact ionization of multicharged ions is explored. [S1050-2947(98)04008-6]

PACS number(s): 34.50.−s, 34.70+e, 52.20.−j

I. INTRODUCTION

In recent years, a considerable effort has been spent to organize and understand the basic ideas and concepts related to dynamic electron-electron correlations in atomic collisions [1–5]. Dynamic correlation involves multiple electronic transitions, and the understanding of these correlations, when many electrons participate, is difficult both from the theoretical and experimental points of view. For that reason, there is a demand for studying simpler collision systems, where these correlations are restricted to two-electron transitions. In the case of one-center correlation [1], where the two electrons are associated with one of the collision partners, collisions of bare ions with He targets are the natural choice to study this kind of correlation. In the case of two-center correlations [1], where each one of the two electrons is associated with each collision partner, collisions of one-electron projectiles with atomic hydrogen are the most convenient systems to limit the correlation to two electrons only. This is an important virtue of atomic hydrogen targets, not mentioned in the literature. Indeed, atomic hydrogen has been used mostly to study collision systems without or ignoring dynamic correlations.

One important feature of the two-center correlation associated with electron loss, also called antiscreening [3], is that it has an effective threshold at intermediate velocities, which makes measurements in the intermediate-to-high velocity region essential to study this mechanism. However, there are very few experimental data with atomic hydrogen targets in this velocity regime with even less absolute measurements among them. For example, the He^+ electron loss data of Hvelplund and Andersen [6] and the He^+ electron loss data of Shah *et al.* [7] were normalized by the He^{2+} capture data of Shah *et al.* [8], which, in turn were normalized by absolute electron capture measurements by protons of McClure [9]. A similar scenario holds for C^{3+}, another projectile studied in this work.

Due to the practical impossibility to obtain pure atomic hydrogen targets, absolute measurements involving H atoms are performed by means of the measurement of the ratio σ_{H_2}/σ_H. This ratio also explores the differences in electron loss due to the molecular nature of H_2 when compared with H.

Meyerhof *et al.* [10] showed that the H_2 molecular form factor affects in different ways the screening and the antiscreening contributions to electron loss. The ratio σ_{H_2}/σ_H is particularly sensitive to the way in which the interference caused by the two nuclei of the H_2 molecule is modeled by the calculations. This sensitivity of the electron loss cross section to the molecular form factor is enhanced for light projectile ions, such as the He^+ studied in this work.

A further step in studying two-center electron-electron correlation is to consider this interaction when other collision channels occur concomitantly. This happens in collisions involving multiply charged ions and neutral targets, a situation explored in this work by using C^{3+} projectiles. In the collision regime studied here, essentially only the $2s$ electron of the C^{3+} ion is active and, from this perspective, this system is similar to $He^+ + H^0$, with only two active electrons. However, electron capture becomes relevant for C^{3+} projectiles, requiring two-step processes, such as capture-loss, to be considered in the intermediate-velocity regime. As a consequence, the theoretical analysis becomes more laborious

*Present address: Instituto de Física, Universidade Federal Fluminense, Caixa Postal 38071, Niterói 22452-970, RJ, Brazil.

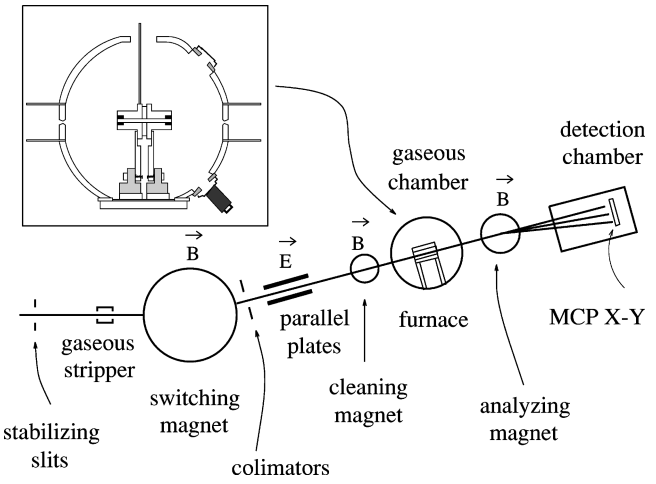

FIG. 1. Sketch of the experimental arrangement; the gas chamber with the hydrogen furnace is in the inset.

compared to the He^+ case. The independent electron approximation (IEA), which has been successfully used in several collisions systems and at different velocity regimes [2], is used to interpret the experimental data. From this analysis, the possibility to make a direct comparison between measurements of electron loss and of electron impact ionization of multiply charged ions is shown, building a bridge between these two apparently dissociated branches of atomic-collision physics.

This paper is organized as follows: in Sec. II, the experimental arrangement and procedures are described and the measurements are presented. In Sec. III, the experimental σ_{H_2}/σ_H ratios for electron loss are compared with various theoretical approximations, taking into account the screening and antiscreening contributions to the H_2 form factors. In Sec. IV, the interconnection between electron loss and electron impact ionization is discussed for He^+ projectiles. In Sec. V, the measured cross sections for C^{3+} electron loss are compared with theoretical calculation based on the IEA, considering the screening and antiscreening contributions to electron loss, as well as the electron capture, target ionization and transfer-loss channels. In Sec. VI, a summary of the work is presented.

II. EXPERIMENT

A general sketch of the experimental arrangement is shown in Fig. 1. Singly-charged He^+ or C^+ beams with energies between 0.5 and 3.5 MeV are delivered by the 4-MV Van de Graaff accelerator of the Catholic University of Rio de Janeiro. After being charge and energy analyzed, the selected beams enter the experimental line through the switching magnet. The higher charge state C^{3+} beams are obtained by a gaseous stripper placed just before the switching magnet. The He^0, He^+, and C^{3+} beams are collimated by a 0.2-mm-diameter aperture, pass through an electrostatic deflector, a cleaning magnet, and enter the scattering chamber. A 4-kV/cm electric field is applied in the electrostatic deflector, 30 cm long, if the He^0 beam is used. The cleaning magnet, located at ~ 0.2 m from the center of the scattering chamber, makes the final charge state selection and eliminates undesirable contributions from beam contamination and charge-exchange collisions in the beam line which is kept at a pressure below 10^{-6} Torr. After passing through the gas chamber, which houses the atomic hydrogen furnace, the emergent beam is charge-analyzed by the analyzing magnet and impinges on the x-y position-sensitive channel-plate detector placed in the detection chamber located ~ 4.5 m downstream. This detector also allows a proper spatial separation of the spurious beams split by the cleaning magnet. To obtain a clear separation of the spurious beams when the atomic hydrogen furnace is working the main beam must be properly focused in order to obtain a small spot size on the x-y detector. The high electric current of the furnace deforms the beams passing through the gas cell and significantly enlarges the spot sizes in the x-y detector compared with those obtained with the furnace off. Although the results for electron capture are not reported here, this channel was also measured to correctly account for the conservation of the particle flux. This is an important point mainly for C^{3+}, where electron capture is a major charge-changing channel for this projectile.

The furnace design as well as its absolute calibration are described in greater detail elsewhere [11] and only the major points of the setup and calibration procedure are recalled here (see inset of Fig. 1). The furnace is made of a tungsten sheet 0.025 mm thick, 8.0 cm long and 3.7 cm wide rolled in a tube-shaped form with 5.3 mm external diameter which is held at the ends by two molybdenum caps. The later are held by two water-cooled copper pieces which provides the proper refrigeration of the furnace, as well as allowing a supply of 110 A ac electric current to heat the tungsten tube up to 2600 K. The large radiative heat transfer from the tungsten cell to the surroundings causes thermal desorption from almost all surfaces in the gas chamber. Careful surface cleaning and efficient vacuum pumping is thus needed to keep the system clean of impurities during the furnace operation. During normal operation, at 2600 K, the pressure in the gas chamber was kept below 1.0×10^{-6} Torr or 3.0×10^{-6} Torr, without or with H_2 feeding, respectively. The molecular hydrogen is fed into the center of the tungsten cell through a second tungsten tube with 2 mm diameter and eventually makes a dissociative reaction with the hot walls of the cell. The final mixture of H and H_2 in the cell is a result of the balance between the dissociation and recombination processes in the confining hot walls.

Since the recombination process cannot be eliminated completely in practice, collision experiments using this type of furnace have to be done in a H plus H_2 mixture. As a consequence, the relative number density of both gases along the projectile beam path needs to be known and only the ratio between the cross sections for H and H_2 targets can be obtained in this kind of measurement.

The procedure used in the calibration, as well in the measurements performed in this work, are based on the two-temperature method [11,12]. For a generic collision channel, the corresponding yields at $T_0=1400$ K, when only H_2 is present, and at $T=2600$ K, when the target gas is highly dissociated, are measured keeping the same gas inflow. Denoting these yields by $S(T_0)$ and $S(T)$, respectively, it can be shown that the ratio σ_H/σ_{H_2} of the corresponding cross sections for H and H_2 targets is given by [11,12]

$$\frac{\sigma_H}{\sigma_{H_2}} = \frac{1-D(T)}{D(T)}\left[\frac{1}{f(T,T_0)}\frac{S(T)}{S(T_0)} - 1\right], \quad (1)$$

where $D(T)=n_H(T)/[n_H(T)+n_{H_2}(T)]$ is the degree of dissociation, and $f(T,T_0)=n_{H_2}(T)/n_{H_2}(T_0)$ is the dissociation fraction. The parameters $n_H(T)$ and $n_{H_2}(T)$ denote the number densities, at the indicated temperature, of the H and H_2 fractions present in the cell, respectively. The furnace is calibrated by determining $f(T,T_0)$ and $D(T)$ as a function of the furnace current.

The dissociation fraction was determined through the measurement of the double capture by C^{3+} projectiles at 1.1 MeV. Because $\sigma_H=0$ for the double capture channel, the term between brackets in Eq. (1) is equal to zero. This gives directly $f(T,T_0)$ from the measured ratio between the double-capture yields at the temperatures T and T_0. For the temperature pairs $T_0=1400$ K and $T=2600$ K, a dissociation fraction of 0.165 ± 0.005 was obtained. The absolute value for the degree of dissociation was obtained through the measurement of the angular distribution of elastically-scattered 1.0 MeV He^0 projectiles impinging on the *x-y* position-sensitive detector (see Fig. 1), within the angular range between 0.2 and 0.6 mrad. Using the measured constant values of the elastic scattering yields, $\theta^4 d\sigma_{elastic}/d\theta$, for $S(T)$ and $S(T_0)$, $D(T)$ can be directly obtained from Eq. (1) by noting that for elastic scattering $\sigma_H/\sigma_{H_2}=1/2$. For $T=2600$ K a degree of dissociation of 0.80 ± 0.02 was obtained [11].

The electron loss cross sections for atomic hydrogen are obtained from Eq. (1) together with the measurement, at the same projectile energy, of the electron loss cross section in H_2, at room temperature. The experimental arrangement is similar to that described in Ref. [13], except that the emergent beams are now detected by the *x-y* position sensitive detector and the cleaning magnet placed before the scattering chamber allows an easier elimination of the spurious beams. The cross sections are obtained by the growth-rate method with the pressure in the gas cell measured by an absolute capacitive manometer (MKS-Baratron). With this setup the main sources of uncertainties come from gas purity ($\sim$1–3 %), reproducibility of the oven temperature ($\sim$1%), counting statistics ($\sim$5%), interference of spurious beams ($\sim$1%) and, for the H_2 measurements, the determination of the effective length of the cell ($\sim$5%).

Table I shows our experimental results for the He^+ and C^{3+} projectiles. Our present measurements for H_2 targets are in very good agreement with previous experimental results of Shah *et al.* [7], Sataka *et al.* [14], and Montenegro *et al.* [15] in the case of He^+ projectiles, and with the results of Montenegro *et al.* [13] and Goffe *et al.* [16] for C^{3+} projectiles. The above set of measurements for He^+ is also in good agreement with recent PWBA calculations of Refs. [10] and [18], indicating a consistent description of He^+ electron loss on molecular hydrogen, as will be discussed in greater detail in the next section. It should be mentioned that the He^+ measurements of Pivovar *et al.* [17] and Hvelplund and Andersen [6] on H_2 also covers the energy range studied in this paper but, as noted by the last authors, their data appear to lie below the theoretical predictions when the projectile energy increases, a tendency which is confirmed by the present measurements.

TABLE I. Electron-loss cross sections for He^+ and C^{3+} impact on H and H_2. All cross sections in Mb.

E (MeV)	He^+		C^{3+}	
	H_2	H	H_2	H
0.50	20.6 ± 0.8	14.8 ± 1.4		
0.75	20.7 ± 0.9	10.8 ± 1.0		
1.00	21.0 ± 0.9	9.7 ± 0.9	8.0 ± 0.8	
1.10			8.8 ± 0.8	7.5 ± 1.0
1.25	19.7 ± 1.1	9.3 ± 0.9		
1.38			9.8 ± 1.1	
1.50	17.5 ± 0.9	8.6 ± 0.8	11.2 ± 1.1	7.2 ± 0.9
1.75	17.9 ± 0.9	7.5 ± 0.7	12.2 ± 1.2	7.3 ± 0.9
2.00	16.4 ± 0.8	7.8 ± 0.7	13.4 ± 1.1	7.8 ± 0.9
2.25	15.0 ± 0.6	6.9 ± 0.6	13.9 ± 1.0	6.7 ± 0.7
2.50	13.6 ± 0.7	6.5 ± 0.6	15.6 ± 1.1	7.6 ± 0.8
2.75	12.1 ± 0.7	5.8 ± 0.6	14.1 ± 1.0	6.2 ± 0.6
3.00			14.9 ± 1.7	7.2 ± 1.0
3.25			15.8 ± 2.1	8.4 ± 1.3
3.50	10.3 ± 0.9	4.8 ± 0.6	13.9 ± 1.8	7.4 ± 1.2

III. MOLECULAR EFFECTS ON ELECTRON LOSS

As shown by Meyerhof *et al.* [10], the ratio σ_{H_2}/σ_H of the electron loss cross sections of light projectiles on H_2 and H targets is very sensitive to the way the molecular form factor is modeled in the calculations of the electron loss cross sections. These calculations take into account two competing mechanisms which contribute to the loss process in the intermediate-to-high velocity regime: the correlated electron-electron interaction between the target electrons and the active projectile electron (*antiscreening mode*) and the Coulomb interaction between the screened target nucleus (or nuclei, in the case of molecular targets) and the active projectile electron (*screening mode*). For He^+ projectiles within the energy range covered by this work, the electron-electron contribution is as important as the nucleus-electron interaction, for both H and H_2 targets [3], making the measurement of the ratio σ_{H_2}/σ_H sensitive to the way the molecular form factor contributes in each one of the above-mentioned modes.

Following the notation of Ref. [10], the electron loss cross section can be written in first-order Born approximation (PWBA) as (see also Ref. [3])

$$\sigma_{s,a} = \frac{8\pi}{v^2}\int_0^\infty d\varepsilon \int_{q_{\min(s,a)}}^\infty q^{-3} dq |F_p(q)|^2 S_{s,a}(q), \quad (2)$$

where

$$S_s(q) = \int (4\pi)^{-1} d\Omega_\rho 2[1+\cos(\mathbf{q}\cdot\boldsymbol{\rho})]|1-F_t(q)|^2 \quad (3)$$

and

$$S_a(q)=\int (4\pi)^{-1} d\Omega_\rho \, 2[1+\cos(\mathbf{q}\cdot\boldsymbol{\rho})][1-|F_t(q)|^2] \tag{4}$$

for H_2 targets. For atomic hydrogen, we have

$$S_s=|1-F_0(q)|^2, \tag{5}$$

$$S_a=1-|F_0(q)|^2. \tag{6}$$

In Eqs. (2)–(6), v is the collision velocity, ε is the kinetic energy of the ejected electron, $\mathbf{q}$ is the momentum transferred in the collision, $\boldsymbol{\rho}$ is the internuclear separation of the hydrogen molecule, and $F_p(q)$, $F_t(q)$ and $F_0(q)$ are the projectile, H_2 and H single-electron form factors as given by Eqs. (9), (28), and (30) of Ref. [10], respectively.

In order to analyze the importance of averaging over the molecular orientations in the interference term appearing in Eqs. (3) and (4), Meyerhof *et al.* [10] described three different procedures with increasing degrees of simplification. In the ''Weinbaum'' model, the Weinbaum wave function for H_2 is used to calculate the form factor $F_t(q)$, and then $S_{s,a}(q)$ through Eqs. (3) and (4). In the ''Stewart'' model, a form factor which is already orientation-averaged is used, so that the interference term appearing in Eqs. (3) and (4) can be calculated independently and a simpler analytical result is obtained for $S_{s,a}(q)$. Besides these two models from Ref. [10], we also use in the forthcoming discussion a further simplified model — hereafter denominated ''Simpl'' model — in which the H_2 molecule is modeled as two hydrogen atoms but with the hydrogenic form factor $F_0(q)=1/[1+(q/2Z_{\rm eff})^2]^2$ calculated using an effective charge $Z_{\rm eff}=1.193$, as given by the Weinbaum model.

For the screening mode we used $q_{\min(s)}=q_0=I_p/v$ as usual [10,18], with I_p being the ionization energy of the active projectile electron. Our present calculations differ from those in Ref. [10] with respect to the antiscreening mode. For the antiscreening mode, Meyerhof *et al.* [10] used the *ad hoc* prescription by Anholt [19] where the value of the energy transfer appearing in $q_{\min(a)}$ is averaged over the possible energies transferred to the continuum states of the projectile and the target, and the cross section given by Eq. (2) is modeled as the ionization cross section of the projectile ion by electrons with the same velocity. In the present paper we use a generalization, for molecular targets, of the extended sum-rule method of Montenegro and Meyerhof [18], thus keeping the calculation consistently within the PWBA. This generalization is carried out by using an orientation-averaged molecular form factor in the calculation of $q_{\min(a)}$. Using the same procedure as described in Ref. [18] it is straightforward to obtain

$$q_{\min(a)}=q_0+\Delta q(q_0+\Delta q(q_0)), \tag{7}$$

where

$$\Delta q(q)=\frac{q^2/2v}{1-\overline{F_t^2(q)}}, \tag{8}$$

with

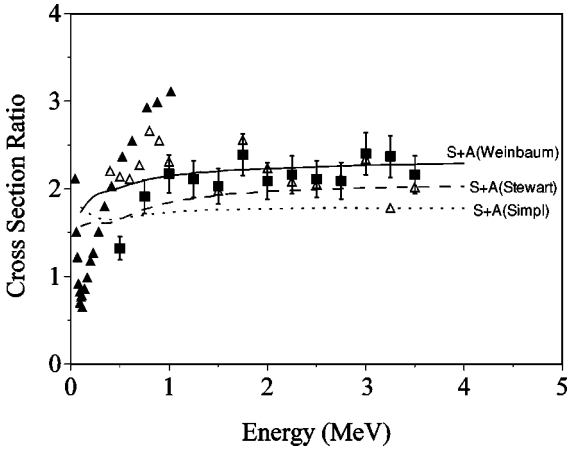

FIG. 2. Cross section ratio σ_{H_2}/σ_H for electron loss of He^+ projectiles as function of the projectile energy. Experiment: solid squares, this work; solid triangles, Ref. [7]; open triangles, Ref. [6]. Theory: solid curve, Weinbaum model; dashed curve, Stewart model; dotted curve, Simpl model (see text).

$$\overline{F_t^2}(q)=[g(q)F_0(q)]^2[2a^2(1+R_2(q))+b^2+4abR_1(q)]$$

for the Weinbaum model and

$$\overline{F_t^2}(q)=[g(q)F_0(q)]^2$$

for the Stewart model. The reader is referred to Ref. [10] for the definitions of these parameters and functions.

Figure 2 shows our measurements of the σ_{H_2}/σ_H ratio for He^+ electron loss compared with those of Hvelpund and Andersen [6] and Shah *et al.* [7], together with the present calculations corresponding to the three models described above. Our measurements show a good agreement with the previously measured data, although, as mentioned in the introduction, none of the previous measurements is absolute. For projectile energies above $\sim$1.0 MeV, the experimental data lie between the results from the Weinbaum and Stewart model calculations, with the Weinbaum model giving a slightly better agreement. The Simpl model underestimates the experiment by $\sim$16% in this energy range.

A detailed evaluation of the role played by the molecular structure in the screening and antiscreening modes can be seen from Fig. 3 where the contributions from the various models to σ_{H_2}/σ_H are split. Besides the present experimental results, Fig. 3 also shows the separate contribution from antiscreening, $\sigma^A_{H_2}/\sigma_H$. The latter is obtained through the expression

$$\frac{\sigma^A_{H_2}}{\sigma_H}=\left(\frac{\sigma^A_{H_2}}{\sigma_{H_2}}\right)\left(\frac{\sigma_{H_2}}{\sigma_H}\right), \tag{9}$$

where the term $\sigma^A_{H_2}/\sigma_{H_2}$ is taken from the coincidence measurements of Ref. [15] and the term σ_{H_2}/σ_H from the present measurements. The coincidence data include a contribution from the two-step loss-ionization process. This contribution, however, decreases rapidly from $\sim$25% at 1.5 MeV to $\sim$10% at 3.5 MeV [15].

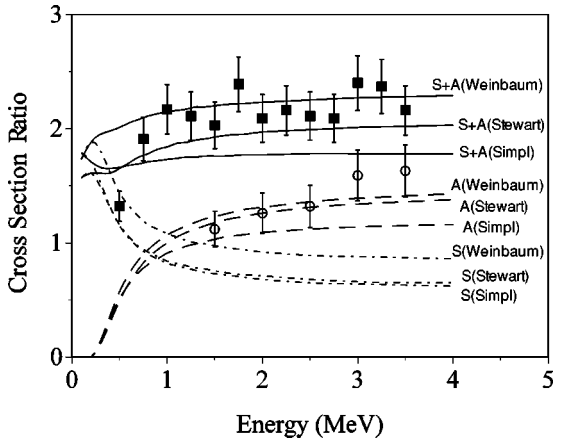

FIG. 3. Cross section ratio σ_{H_2}/σ_H for electron loss of He^+ projectiles as function of the projectile energy. The screening (S) and antiscreening (A) contributions associated with the Weinbaum, Stewart, and Simpl models are split from the total (S+A) contributions. Experiment: solid squares, this work; open circles, ratio for the antiscreening contribution [see Eq. (9)].

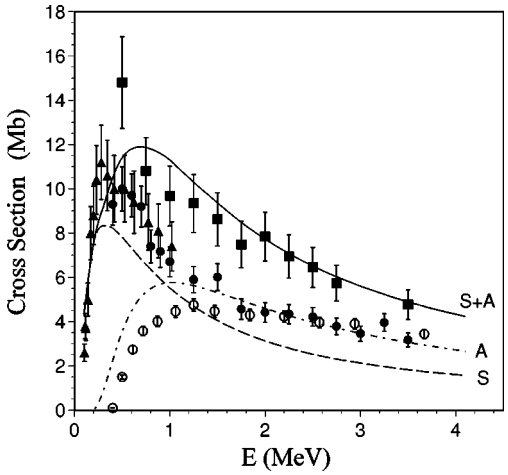

FIG. 4. Cross section for electron loss of He^+ projectiles on atomic hydrogen. Experiment: solid squares, this work; solid circles, Ref. [6]; solid triangles, Ref. [7]; open circles, electron-impact ionization of He^+ from Ref. [27]. Theory: dashed curve, screening; dashed-dotted curve, antiscreening; solid curve, total cross section for electron loss. The antiscreening calculations are based on the PWBA extended sum-rule method of Ref. [18].

As Fig. 3 shows, the Simpl model gives a description of the singles and coincidence data which is clearly smaller than the Weinbaum and the Stewart models. The main difference between the Simpl and the two other models is that the former ignores the interference caused by the joint action of the two nuclei in the projectile ionization process. This shows that the contribution from the interference is indeed important, coming principally from the antiscreening mode. This result can be understood if we note that the major contribution to the $\cos(\mathbf{q}\cdot\boldsymbol{\rho})$ term in Eqs. (3) and (4) comes from small values of the momentum transferred to the active projectile electron, q. For small values of q, the argument $\mathbf{q}\cdot\boldsymbol{\rho}$ oscillates slowly and the contribution from this term is large. However, small values of q correspond to large impact parameters for which the antiscreening contribution dominates [3]. If q is large, $\mathbf{q}\cdot\boldsymbol{\rho}$ oscillates rapidly and the contribution from the interference term is small. This corresponds to close collisions where the screening mode dominates [3], thus explaining why the Simpl model gives a ratio which is close to the Stewart model for the screening mode (Fig. 3).

IV. TOTAL ELECTRON LOSS ON H: ANTISCREENING, IMPULSE APPROXIMATION, AND CONNECTION WITH ELECTRON-ION COLLISIONS

As mentioned in Sec. II, the total electron loss cross section of He^+ on atomic hydrogen can be obtained from the measurement of the ratio σ_{H_2}/σ_H together with the absolute measurements on H_2 targets. Figure 4 compares the electron loss results thus obtained (Table I) with those of Hvelplund and Andersen [6], Shah *et al.* [7] as well as with the PWBA calculations as described in Sec. III. As a general trend, the results from the PWBA calculations agree well with our data, particularly in the high energy region. These calculations show a broad maximum for projectile energies around 800 keV, which is essentially due to the onset of the antiscreening contribution, a behavior which was already indicated by the early calculations of Bell and Kingston [21]. This behavior contrasts with the data from Refs. [6] and [7], which point towards a sharp maximum for projectile energies around 300 keV. Although our data cannot give a clear answer about the shape of the cross section near the maximum, it should be noted that if the data of Refs. [6] and [7] are multiplied by a factor ~ 1.45, there is a quite good agreement between the three sets of data.

The role of the antiscreeening contribution to the total electron loss cross section can be advantageously examined with the aid of the impulse approximation [3,4,22]. If we consider that only continuum states of the target contribute to the electron-electron interaction, it can be shown that the cross section for the antiscreening contribution can be written as [3,4,22]

$$\sigma_a^{\mathrm{imp}} = \int_{-\infty}^{+\infty} dv_z \sigma_e(v+v_z) J(v_z). \tag{10}$$

The above equation can be pictured, in the projectile frame, as the ionization of the projectile ion by a beam of electrons with a velocity $v+v_z$ broadened by the Compton profile $J(v_z)$ of the target ground state. This expression, apart from giving an useful intuitive physical picture of the electron-electron interaction, makes an important connection between the antiscreening cross section, σ_a^{imp}, and the ionization cross section of multiply charged ions by electron impact, $\sigma_e(v+v_z)$. This connection can be made even more explicit if we recall that the atomic hydrogen ground state has a sharp Compton profile around $v_z=0$ [4]. In fact, outside the threshold region, where $\sigma_e(v+v_z)$ varies rapidly with v_z, the velocity dependence of $\sigma_e(v+v_z)$ is smooth enough to be considered constant within the velocity range where the Compton profile is significant. Under these conditions we can make the assumption

$$\sigma_a^{\mathrm{imp}} \simeq \sigma_e(v), \tag{11}$$

obtaining a direct relationship between these two cross sections. The validity of this equation was recently verified through electron loss experiments involving highly charged ions and He targets using the recoil ion momentum spectroscopy technique [23–26]. With this technique, the screening and antiscreening modes can be separated, allowing a direct comparison of the antiscreening contribution with theoretical calculations of ionization of highly charged ions by electron impact or experiments using crossed or merged electron-ion beams.

On the basis of the above analysis, we can use electron-ion measurements to evaluate the antiscreening contribution to our measured total cross section for electron loss. To this end, Fig. 4 displays the $e+He^+$ ionization cross section measurements of Peart *et al.* [27]. There is a good agreement between the electron data and our present antiscreening calculations, indicating a general consistency between theory and the present measurements in this case. Since the convergent close-coupling calculations for the $e+He^+$ ionization cross section by Bray *et al.* [28] are in excellent agreement with the measurements of Ref. [27], they can also be used, within the impulse approximation, to estimate the antiscreening contribution.

V. TOTAL ELECTRON LOSS ON H: THE ROLE OF THE CAPTURE AND IONIZATION CHANNELS

In the case of C^{3+} projectiles, where the projectile charge state is higher and the velocity is lower than in the He^+ case studied above, target ionization and electron capture become the major collision channels in the velocity regime studied in this work. Under these circumstances, to describe properly the electron loss process, it is necessary to include in the theoretical models not only the effects due to these channels, but also the increased possibility of multielectronic transitions and the nonperturbative character acquired by the collision.

Simple models based on first-order calculations which incorporate some *non–ad hoc* procedure to force the necessary unitarization for the set of participating channels have been used successfully to interpret the experimental results of some complex collisions involving highly charged ions, such as, for example, the ratio between the transfer-ionization and the single capture channels of 1-MeV/amu Ti^{18+} projectiles impinging on He [29]. In this paper we use the procedure given by Sidorovich *et al.* [30] in a similar fashion as used in Ref. [29].

Let us denote by $p_I(b)$ and $p_C(b)$ the probabilities, as functions of the impact parameter b, for the target H electron to be ionized or to be captured, respectively. These probabilities are independently calculated through first-order theories. We exclude the target excitation channel because it can be neglected when compared to target ionization in the impact parameter region where electron capture is important [29]. Following Ref. [30], the unitarized probability $P_\alpha(b)$, where α denotes I or C, is given by

$$P_\alpha(b)=\frac{p_\alpha(b)}{p_I(b)+p_C(b)}[1-e^{-(p_I(b)+p_C(b))}]. \qquad (12)$$

The probability $p_C(b)$ is calculated according to the model of Ben-Itzhak *et al.* [31]. The target ionization probability is calculated through the equation $p_I(b)=Q^2p_{\rm sca}(b)$, where $p_{\rm sca}(b)=|a^{1s}_{\rm sca}(b)|^2$ is the semiclassical calculation for the ionization probability of the $1s$ electron of H by protons, taken from Ref. [32], and $Q=3$ for C^{3+} projectiles.

Because the antiscreening mode results mostly in the simultaneous ionization of the projectile active electron and the target electron, the only possibility for electron capture to occur concomitantly with electron loss is through the screening mode. Thus, if we denote by $P_{\rm screen}(b)$ and $P_{\rm anti}(b)$ the probabilities of electron loss through the screening and antiscreening modes, respectively, the probability for single electron loss (SL) is given, within the IEA, as

$$P_{\rm SL}(b)=P_{\rm screen}(b)[1-P_C(b)]+P_{\rm anti}(b), \qquad (13)$$

which, integrated over impact parameter gives:

$$\sigma_{\rm SL}=\sigma_{\rm screen}-\sigma_{\rm TL}+\sigma_{\rm anti}, \qquad (14)$$

where $\sigma_{\rm TL}$ is the cross section for the transfer-loss channel. The probability $P_{\rm screen}(b)$ which appears in the calculation of the transfer-loss cross section is evaluated following the lines indicated in Refs. [3,20,33] as

$$P_{\rm screen}(b)=\left|a^{2s}_{\rm sca}(b)-\frac{a^4}{2\gamma}\left\{\int_0^b[bI_0(\gamma x)K_1(\gamma b)-xI_1(\gamma x)K_0(\gamma b)]a^{2s}_{\rm sca}(x)xdx+\int_b^\infty[xI_0(\gamma b)K_1(\gamma x)-bI_1(\gamma b)K_0(\gamma x)]a^{2s}_{\rm sca}(x)xdx\right\}\right|^2, \qquad (15)$$

with $\gamma=[(\omega/v)^2+a^2]^{1/2}$ and K_0, K_1, I_0, and I_1 being modified Bessel functions. In atomic units, $a=2$, v is the projectile velocity and ω is the energy transferred to the $2s$ electron during the ionization of the C^{3+} projectile ion. As in the He^+ case, the cross sections $\sigma_{\rm screen}$ and $\sigma_{\rm anti}$ are calculated within the PWBA using the extended sum-rule method of Ref. [18].

Figure 5 shows our measurements together with the measurements of Goffe *et al.* [16] for C^{3+} projectiles. There is a good agreement between the two sets of data in the energy region where measurements overlap, with the present measurements indicating a broad maximum for the electron loss cross section. In order to better analyze the role played by the various collision mechanisms in the total cross section, the theoretical calculations are split into their corresponding contributions. The basic mechanisms are essentially the same as those appearing in the He^+ case, i.e, the screening plus antiscreening contributions. This joint contribution is shown by the dashed-double dotted curve. However, as indicated in Eq. (14), this curve must be corrected to account for the presence of transfer loss. The transfer-loss contribution (dotted curve) is more important at energies below the maximum of the screening contribution (long-dashed curve), giving a rapidly decreasing contribution at higher energies, where the antiscreening contribution (dashed-dotted curve) becomes impor-

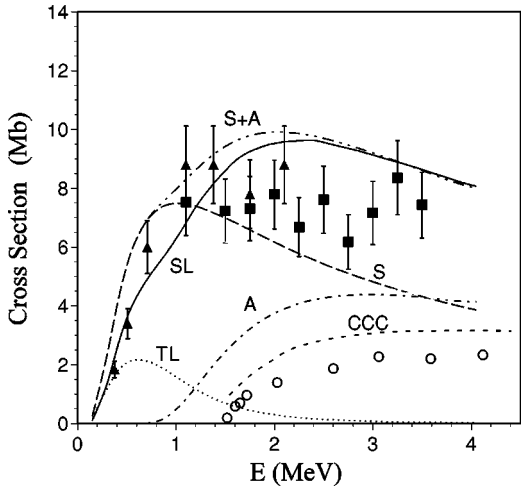

FIG. 5. Cross section for electron loss of C^{3+} projectiles on atomic hydrogen. Experiment: solid squares, this work; solid triangles, Ref. [16]; open circles, electron-impact ionization of C^{3+} from Ref. [34]. Theory: long-dashed curve, screening; dashed-dotted curve, antiscreening; dashed-double dotted curve, screening plus antiscreening; dotted curve, transfer-loss (see text); solid curve, total cross section for single electron loss. The antiscreening calculations are based on the PWBA extended sum-rule method of Ref. [18]. The short-dashed curve is the convergent close-coupling calculation of Ref. [35] for electron-impact ionization of C^{3+}.

tant. The resulting sum of all contributions is shown by the full curve, which gives a good description of the trend of the experimental data but overestimates it by $\sim 20\%$ around the cross section maximum.

As mentioned above, the transfer-loss process has a negligible influence over the electron loss cross section for projectile energies above the onset of the antiscreening channel. Then, $\sigma_{SL} \simeq \sigma_{screen} + \sigma_{anti}$ and the analysis used in the previous section, based on the impulse approximation, can serve to understand better the contribution from the antiscreening mode. Following Eq. (11), we can use electron impact ionization of C^{3+} to account for the antiscreening contribution. These results are also shown in Fig. 5: the open circles are the measurements of Crandall *et al.* [34] and the short-dashed curve is the convergent close-coupling calculations of Bray [35] for the $e + C^{3+}$ ionization.

It is clear from this figure that the good agreement between the electron-impact ionization and the antiscreening cross sections obtained in the He^+ case is not repeated in the C^{3+} case. Indeed, the experimental $e + C^{3+}$ data is almost a factor of 2 smaller than the PWBA antiscreening calculation. As pointed out by Montenegro and Zouros [22], there is a tendency for the impulse approximation to give lower values than the PWBA extended sum rule for the electron-electron contribution because of the averaging procedure used to set the minimum momentum transfer. Although the impulse approximation discards the possibility of excitation for the target electron, this limitation seems to be less important than the need of an averaging procedure for the minimum momentum transfer in the sum-rule method and the results from the impulse approximation are, in general, in better agreement with the experiment [4,22,25]. This behavior appears to be the same here: if we add the $e + C^{3+}$ experimental results to the calculated screening contribution we obtain a very good agreement with the measured C^{3+} electron loss cross section. The $e + C^{3+}$ convergent close-coupling calculations of Bray [35] present the same trend of the experimental electron-ion ionization over this energy region. However, because it overestimates the experimental electron-ion data, it also gives slightly higher values for the total electron loss cross section if added to the calculations for the screening contribution.

VI. SUMMARY AND CONCLUSIONS

The purpose of this paper is threefold. First, to obtain absolute experimental data of the electron loss cross section for He^+ and C^{3+} projectiles on atomic hydrogen in the intermediate-to-high velocity regime, above the onset of the antiscreening mode. This was achieved through the combination of an absolutely calibrated atomic hydrogen furnace together with the measurement of small-angle elastic scattering to determine the number density of the protons inside the furnace.

Second, to show how the electron loss cross section is affected by the different ways the H_2 form factor is modeled. We find that the interference term associated with the two protons of H_2 plays a major role in the calculation of the electron loss cross section, particularly at large impact parameters where the antiscreening mode is dominant. The Weinbaum model, which is the more refined model used in this work, gives a very good agreement with the experimental data in the intermediate-to-high velocity region.

Third, we explore the connection between the antiscreening mode and the ionization of multicharged ions by electron impact. This connection is based on the impulse approximation and forms an important bridge between two different areas of atomic collision physics. We find that a significant improvement in the agreement between experiment and theory is obtained if the electron-electron contribution to the total electron loss is computed directly by means of the cross sections for electron impact ionization of the projectile.

ACKNOWLEDGMENTS

This work was supported in part by the Brazilian Agencies CNPq, FINEP, CAPES, FAPERJ, and MCT (PRONEX).

[1] N. Stolterfoht, in *Spectroscopy and Collisions of Few-Electron Ions*, edited by M. Ivascu, V. Florescu, and V. Zoran (World Scientific, Singapore, 1989), pp. 342–393.

[2] J. H. McGuire, Adv. At., Mol., Opt. Phys. **29**, 217 (1992).

[3] E. C. Montenegro, W. E. Meyerhof, and J. H. McGuire, Adv. At., Mol., Opt. Phys. **34**, 249 (1994).

[4] T. J. M. Zouros, Comments At. Mol. Phys. **32**, 291 (1996).

[5] J. H. McGuire, *Electron Correlation Dynamics in Atomic Col-*

lisions (Cambridge University Press, New York, 1997), Sec. 1-10.
[6] P. Hvelplund and A. Andersen, Phys. Scr. **26**, 370 (1982).
[7] M. B. Shah, T. V. Goffe, and H. B. Gilbody, J. Phys. B **10**, L723 (1977).
[8] M. B. Shah and H. B. Gilbody, J. Phys. B **11**, 121 (1978).
[9] G. W. McClure, Phys. Rev. **148**, 47 (1966).
[10] W. E. Meyerhof, H.-P. Hülskötter, Q. Dai, J. H. McGuire, and Y. D. Wang, Phys. Rev. A **43**, 5907 (1991).
[11] M. M. Sant'Anna, W. S. Melo, A. C. F. Santos, G. M. Sigaud, E. C. Montenegro, W. E. Meyerhof, and M. B. Shah, Nucl. Instrum. Methods Phys. Res. B **132**, 306 (1997).
[12] M. B. Shah and H. B. Gilbody, J. Phys. B **7**, 630 (1974).
[13] E. C. Montenegro, G. M. Sigaud, and W. E. Meyerhof, Phys. Rev. A **45**, 1575 (1992).
[14] M. Sataka, A. Yagishita, and N. Nakai, J. Phys. B **23**, 1225 (1990).
[15] E. C. Montenegro, W. S. Melo, W. E. Meyerhof, and A. G. de Pinho, Phys. Rev. A **48**, 4259 (1993).
[16] T. V. Goffe, M. B. Shah, and H. B. Gilbody, J. Phys. B **12**, 3763 (1979).
[17] L. I. Pivovar, M. T. Novikov, and V. M. Tubarev, Sov. Phys. JETP **15**, 1035 (1962).
[18] E. C. Montenegro and W. E. Meyerhof, Phys. Rev. A **43**, 2289 (1991).
[19] R. Anholt, Phys. Lett. A **144**, 126 (1986).
[20] E. C. Montenegro and W. E. Meyerhof, Phys. Rev. A **46**, 5506 (1992).
[21] K. L. Bell and A. E. Kingston, J. Phys. B **11**, 1259 (1978).
[22] E. C. Montenegro and T. J. M. Zouros, Phys. Rev. A **50**, 3186 (1994).
[23] R. Dörner, V. Mergel, R. Ali, U. Buck, C. L. Cocke, K. Froschauer, O. Jagutzki, S. Lencinas, W. E. Meyerhof, S. Nüttgens, R. E. Olson, H. Schmidt-Böcking, L. Spielberger, K. Tökesi, J. Ullrich, M. Unverzagt, and W. Wu, Phys. Rev. Lett. **72**, 3166 (1994).
[24] W. Wu, K. L. Wong, R. Ali, C. Y. Chen, C. L. Cocke, V. Frohne, J. P. Giese, M. Raphaelian, B. Walch, R. Dörner, V. Mergel, H. Schmidt-Böcking, and W. E. Meyerhof, Phys. Rev. Lett. **72**, 3170 (1994).
[25] C. L. Cocke and E. C. Montenegro, Comments At. Mol. Phys. **32**, 131 (1996).
[26] W. Wu, K. L. Wong, E. C. Montenegro, R. Ali, C. Y. Chen, C. L. Cocke, R. Dörner, V. Frohne, J. P. Giese, V. Mergel, W. E. Meyerhof, M. Raphaelian, H. Schmidt-Bocking, and B. Walch, Phys. Rev. A **55**, 2771 (1997).
[27] B. Peart, D. S. Walton, and K. T. Dolder, J. Phys. B **2**, 1347 (1969). See also P. Defrance, F. Brouillard, W. Claeys, and G. Van Wassenhove, *ibid.* **14**, 103 (1981).
[28] I. Bray, I. E. McCarthy, J. Wigley, and A. T. Stelbovics, J. Phys. B **26**, L831 (1993).
[29] E. C. Montenegro, K. L. Wong, W. Wu, P. Richard, I. Ben-Itzhak, C. L. Cocke, R. Moshammer, J. P. Giese, Y. D. Wang, and C. D. Lin, Phys. Rev. A **55**, 2009 (1997).
[30] V. A. Sidorovich, V. S. Nikolaev, and J. H. McGuire, Phys. Rev. A **31**, 2193 (1985).
[31] I. Ben-Itzhak, A. Jain, and O. L. Weaver, J. Phys. B **26**, 1711 (1993).
[32] J. M. Hansteen, O. M. Johnsen, and L. Kocbach, At. Data Nucl. Data Tables **15**, 305 (1975).
[33] E. C. Montenegro and W. E. Meyerhof, Phys. Rev. A **44**, 7229 (1991).
[34] D. H. Crandall, R. A. Phaneuf, and P. O. Taylor, Phys. Rev. A **18**, 1911 (1978).
[35] I. Bray, J. Phys. B **28**, L247 (1995).